



Contents lists available at ScienceDirect

Journal of Magnetic Resonance

journal homepage: www.elsevier.com/locate/jmr

Direct measurement of internal magnetic fields in natural sands using scanning SQUID microscopy



Jan O. Walbrecker^{a,*}, Beena Kalisky^b, Denys Grombacher^a, John Kirtley^c, Kathryn A. Moler^c, Rosemary Knight^a

^aStanford University, Department of Geophysics, 397 Panama Mall, Stanford, CA 94305, USA

^bDepartment of Physics, Nano-magnetism Research Center, Institute of Nanotechnology and Advanced Materials, Bar-Ilan University, Ramat-Gan 52900, Israel

^cStanford University, Center for Probing the Nanoscale, 476 Lomita Mall, Stanford, CA 94305, USA

ARTICLE INFO

Article history:

Received 19 September 2013

Revised 25 January 2014

Available online 5 February 2014

Keywords:

Porous media

Internal magnetic fields

SQUID

ABSTRACT

NMR experiments are ideally carried out in well-controlled magnetic fields. When samples of natural porous materials are studied, the situation can be complicated if the sample itself contains magnetic components, giving rise to internal magnetic fields in the pore space that modulate the externally applied fields. If not properly accounted for, the internal fields can lead to misinterpretation of relaxation, diffusion, or imaging data. To predict the potential effect of internal fields, and develop effective mitigation strategies, it is important to develop a quantitative understanding of the magnitude and distribution of internal fields occurring in natural porous media. To develop such understanding, we employ scanning SQUID microscopy, a technique that can detect magnetic field variations very accurately at high spatial resolution ($\sim 3 \mu\text{m}$). We prepared samples from natural unconsolidated aquifer material, and scanned areas of about $200 \times 200 \mu\text{m}$ in a very low background magnetic field of $\sim 2 \mu\text{T}$. We found large amplitude variations with a magnitude of about 2 mT, across a relatively long spatial scale of about $200 \mu\text{m}$, that are associated with a large magnetic grain ($>50 \mu\text{m}$ radius) with a strong magnetic remanence. We also detected substantial variations exceeding $60 \mu\text{T}$ on small spatial scales of about $\sim 10 \mu\text{m}$. We attribute these small-scale variations to very fine-grained magnetic material. Because we made our measurements at very low background field, the observed variations are not induced by the background field but due to magnetic remanence. Consequently, the observed internal fields will affect even low-field NMR experiments.

© 2014 Elsevier Inc. All rights reserved.

1. Introduction

Proton NMR is a versatile method to characterize fluid-filled porous material. It is employed in various disciplines to study pore-scale properties of porous systems [1], such as in hydrogeophysics to characterize aquifer material [2–9], in the petroleum industry to characterize reservoir rocks [10–14], and in the soil sciences to study water uptake and dynamics in soil [15–20]. These applications primarily rely on measuring the NMR relaxation times, because they are related to important pore-scale properties, such as the surface-area-to-volume ratio of the pore space [21,22]. Another important quantity that can be obtained from NMR measurements is the diffusion coefficient. It can be used for fluid

typing, which is important in petroleum applications to discern water and different types of hydrocarbons [23–25]. Measurement of the apparent diffusion coefficient can provide insight into the geometrical restriction of the diffusion process, which can be used to study pore size and pore geometry [26–28].

In all these NMR relaxometry and diffusometry applications the studied sample is placed in a static background field that is designed to be as homogeneous as possible. In many experimental setups, such as in imaging, pulsed field gradients, or inside-out experiments, additional external magnetic gradients are employed to encode information in the frequency and phase of the NMR signal. Complications can arise when the studied sample itself contains magnetic components. The magnetic components induce a magnetic field that strays into the pore space and modulates the NMR background field. This effect is commonly referred to as internal magnetic field gradients in the pore space, or internal fields, as opposed to the external field gradients generated by NMR tools. Internal fields can arise due to magnetic particles present in the

* Corresponding author.

E-mail addresses: jan.walbrecker@stanford.edu (J.O. Walbrecker), beena@biu.ac.il (B. Kalisky), denysg@stanford.edu (D. Grombacher), jkirtley@stanford.edu (J. Kirtley), kmoler@stanford.edu (K.A. Moler), rknight@stanford.edu (R. Knight).

pore fluid [29], or parts of the solid phase of the sample being magnetic [30–32]. In both cases magnetization is caused by (i) differences in magnetic susceptibility between pore fluid and solid, or (ii) the material carrying magnetic remanence. In case (i) the internal fields can be estimated based on geometry and magnetic susceptibility of the material (if known), and the orientation and magnitude of the NMR background field [33–35]. For case (ii) the situation is more complicated, because the magnetic remanence can have any orientation and magnitude independent of the NMR background field. Note that case (ii), unlike case (i), may occur even in the absence of a background field.

For many applications the effects of internal fields are undesired. If internal fields are not properly accounted for, they can degrade the NMR signal by imposing uncontrolled phase onto the spins during an NMR experiment. This can lead to misinterpretation of pore scale properties due to voxel misplacement in image reconstruction [36], flawed quantification of the relaxation and apparent diffusion parameters [37], or misclassification of characteristic length scales when assessing the diffusion regime [38]. If the internal fields are particularly large, they can shift the Larmor frequency out of the bandwidth of the tuned excitation pulses, such that certain regions in the sample do not contribute to the NMR signal.

Various techniques have been developed to suppress the effects of internal fields. Where possible, experimental parameters are selected such as to minimize the internal field effect. One example is a common Carr–Purcell–Meiboom–Gill (CPMG) measurement of the T_2 relaxation time. The measured T_2 time is related to the surface relaxation T_{2S} , which provides the link to the surface-area-to-volume ratio of the porous system; but it is additionally controlled by the so-called diffusion relaxation T_{2D} , which results from spins diffusing through internal fields during the time between refocusing pulses [39]. This mechanism is commonly described by the equation $T_{2D} = 12/(D_0\gamma^2G^2\tau^2)$, where D_0 is the diffusion constant of water, γ is the proton gyromagnetic ratio, G the average internal field gradient amplitude, and τ the echo spacing in CPMG measurements. Because $1/T_{2D}$ is proportional to τ^2 , minimizing τ therefore increases T_{2D} and thus minimizes the impact of G . But because the minimum echo spacing is technically limited and cannot be made arbitrarily short, this approach will fail if the internal field gradients are very large; considering a minimum echo spacing of $\tau = 1$ ms and an internal field gradient of $G = 1$ T/m yields a T_{2D} of about 106 ms. This is of the same order as typical surface relaxation times (see e.g. [6]) and therefore may bias interpretation of CPMG results.

Other techniques to suppress the effect of internal fields, mainly applied in diffusion measurements, employ stimulated echo techniques which minimize the time the spin magnetization resides in the transverse direction, where it is affected by internal fields [40], or employ pulsed field gradients involving multi-pulse sequences employing bipolar gradients [41–45]. In applications, where such measures to counter the effects of internal fields cannot be employed, such as in borehole NMR, it is sometimes assumed that the (known) external field gradients can be made so large that they dominate the internal fields, thus obliterating their effect [32]. This assumption, however, requires that the magnitude of the internal fields is known, which is often not the case. In a different approach the internal fields are not suppressed, but utilized as a representation of the underlying pore geometry [46]. This technique, known as decay due to diffusion in inhomogeneous fields, has been used to obtain the pore size and pore connectivity in carbonate rocks and sandstones [47,48], and also in medical applications [49–51].

For all these methods, whether designed to suppress or to utilize internal fields, it is important to develop a better understanding of the magnitude and distribution of internal fields that occur

in natural porous media. Yet there are not many published measurements of the internal fields in natural geologic material. In particular, little is known about microscale variations in natural geologic media, although its importance has been recognized [52,53]. Sun and Dunn developed a 2D CPMG sequence to correlate the internal fields with the T_2 relaxation time, demonstrating that higher internal field gradients are associated with regions of smaller pore size [54]. It was noted that this technique may provide only a smoothed representation of the internal fields averaged over the diffusion distance during an NMR experiment [35]. Washburn et al. devised a similar technique to determine the internal field as function of T_1 for different background field amplitudes [55]. They found that the maximum internal field gradient scales as a power law with the amplitude of the background field amplitude. Employing an imaging approach, Cho et al. visualized the internal gradients of a model system of water-filled glass tubes [56]. Complementing these experimental approaches, numerical studies have been undertaken to model internal fields based on optical images taken from natural samples [35,49], or numerically modeled systems [31,34,52,57–59], and using plausible values for magnetic susceptibilities of materials. Numerical approaches typically rely on the assumption that internal fields are caused by differences in magnetic susceptibility and do not include the effect of remanent magnetization.

In our present study we directly quantify the magnitude and spatial distribution of internal fields. We employ high-resolution scanning-SQUID microscopy [60,61] to determine the internal fields that occur in small subsamples taken from natural geologic material. The scanning-SQUID technique maps the magnetic field lines generated by the sample and can give detailed information about magnitude and spatial scale of magnetic variations. Another advantage of this method is that it is independent of NMR, so we avoid complications that may arise when internal fields are strong and occur on small length scales. After briefly introducing the principles of scanning-SQUID microscopy, we describe the samples used for this study, show the measurement results, and discuss the implications our results have for NMR measurements.

2. Materials and methods

2.1. Scanning SQUID microscopy

We use scanning-SQUID microscopy to magnetically image the internal magnetic fields in natural porous geologic material. A superconducting quantum interference device (SQUID) is a sensitive magnetometer composed of a superconducting loop containing two Josephson junctions, illustrated by the red line and red crosses in Fig. 1a. Superconducting materials are characterized by their ability to conduct without resistance (up to a critical current) and to expel magnetic fields (up to a critical field). When an external magnetic field penetrates the superconducting loop, the superconductor generates circulating currents to compensate for the external magnetic field. The DC SQUID is based on the DC Josephson effect, which describes the relation between the supercurrent through a junction and the quantum mechanical phase drop across it. The total phase drop around the loop must be an integer multiple of 2π , and is closely related to the magnetic flux through the loop. When the current in either branch of the SQUID loop exceeds the critical current of its Josephson junction, a voltage appears. The critical current of the SQUID is a periodic function of the flux through the pickup loop, with periodicity of one flux quantum, Φ_0 . If we bias the SQUID above this critical current, we can measure an oscillation in the voltage with the same periodicity, thus obtaining very accurate measurements of magnetic flux.

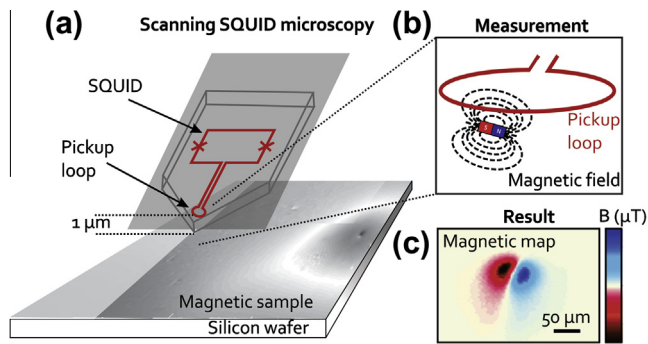


Fig. 1. Scanning SQUID microscopy. (a) The SQUID can be thought of schematically as a superconducting loop with a $3\ \mu\text{m}$ diameter pickup loop (red lines) and two Josephson junctions (red crosses). The SQUID scans over the surface of magnetic sample at an elevation of about $1\ \mu\text{m}$. (b) The magnetic field threading the pickup loop is measured. (c) After scanning the sample surface, the individual measurements are assembled to give a map of magnetic field. (For interpretation of the references to color in this figure legend, the reader is referred to the web version of this article.)

SQUIDS can be designed to be the world's most sensitive flux detectors. The two niobium SQUIDS we used in this work operate at temperatures below $9\ \text{K}$, and are especially designed for scanning, with a gradiometric design to be insensitive to uniform magnetic fields [61]. Each SQUID has a pickup loop of $3\ \mu\text{m}$ diameter. The SQUIDS are operated in a flux locked loop to record the magnetic flux penetrating the pickup loop as a function of position as the device is scanned over the sample surface. The SQUIDS are fabricated on a silicon chip polished to a corner and mounted on a cantilever to bring the pickup loop as close as possible to the sample, see gray frame in Fig. 1a. More details about the SQUID design can be found in [61,62]. When the pickup loop is scanned over a magnetic dipole, it captures the field generated by the dipole at different locations, see Fig. 1b. From the resulting field maps we determine the presence of the dipole, its moment, and orientation [63]. The SQUID can detect nanoscale ferromagnetic objects with moments as small as $10^4\ \mu_B$ in DC, even if they are much smaller than the physical size of the pickup loop. While the technique has unprecedented magnetic sensitivity, it is limited in its spatial resolution. The limitation is due to the pickup loop size and the height above the sample surface, $\sim 1\ \mu\text{m}$ in our setup. Because the measured flux image is a convolution of the magnetic field and the geometric sensitivity of the pickup loop, features that are smaller than $3\ \mu\text{m}$ will be smeared to about $3\ \mu\text{m}$.

An isolated micron- or submicron-scale ferromagnetic patch is conceptually similar to a small bar magnet with physical dimensions that are comparable to or smaller than the pickup loop. In Fig. 1c we illustrate the flux $\Phi(x,y)$ recorded while scanning the SQUID over an isolated magnetic patch such as in Fig. 1b. The size and intensity of the positive and negative lobes (red and blue) depend strongly on the scan height as well as the characteristics of the patch itself. The faint tails to the bottom of the dipole in Fig. 1c are due to flux captured by the unshielded section of the leads to the pickup loop.

2.2. Sample preparation

We prepared 3 samples for our scanning SQUID measurements. Sample 1 was a reference sample consisting of clean quartz Wedron sand with grains of $<100\ \mu\text{m}$ in diameter. The manufacturer specifies $>99.5\%$ silica content, but notes that traces of iron oxide, titanium oxide, and aluminum oxide may occur; of specific relevance to this study is the known occurrence of the magnetic mineral magnetite in the sand. The quartz sand was

magnetically filtered when first received in the laboratory in an attempt to remove any magnetic components but we found, through use of a hand magnet, that some black magnetic grains (presumed to be magnetite) had survived the filtering. The red arrows in the optical microscopy image in Fig. 2a point out some examples of these black-colored grains attached to the light-colored quartz grains.

Samples 2 and 3 consisted of natural sand grains obtained from drill cuttings from a borehole installed at a research site close to Lexington, Nebraska. This site had been developed as part of a research project to monitor the High Plains aquifer, which is one of the US's most important aquifer systems. It has been studied using laboratory, logging, and surface-based NMR methods [8,9,64]. Our sample material was retrieved from a depth of about $23\ \text{m}$. Of relevance to this study is the presence of two types of grains in the sample material—lighter colored grains found to be nonmagnetic and presumed to be quartz, and darker-colored grains found from testing with a hand magnet to be magnetic. We presume that these black grains in the natural sand are magnetite, which is very common in the near surface [65]. For the samples we extracted grains of $<300\ \mu\text{m}$ in diameter, which is typical for fine-grained sand. For sample 2, we used a random mix of grains extracted from the natural sand. For sample 3, we avoided, to the extent possible, including the dark-colored grains and extracted only light-colored grains from the sand. For all samples, the grains were mixed with nonmagnetic epoxy, which we presume would act the same way as pore water devoid of magnetic components. The grains were glued to a silicon wafer by curing the epoxy for $15\ \text{min}$ at 373°K . After the samples had cooled down to room temperature, we polished the sample surfaces using nonmagnetic $0.5\ \mu\text{m}$ polishing paper. Any loose residue was cleaned from the sample surfaces using a nitrogen blower. Optical microscopy images of the samples 2 and 3 (after preparation) are shown in Fig. 2b and c, respectively. We show two images for each sample, one in low resolution with color information, one in higher resolution without color information. Rectangular region 1 of sample 2 is the area covered by scanning SQUID. Because we are primarily interested in NMR experiments that probe water in the pore space of geologic materials, we will focus in our data analysis on a part of the pore space and the pore boundary, marked as rectangle 2. The rectangular region shown for sample 3 is the area covered by scanning SQUID.

For scanning SQUID imaging, the samples were cooled to liquid He temperature, about $4\ \text{K}$. Because (i) the purpose of our measurements is to analyze the internal magnetic field at room temperature, at which NMR experiments are typically carried out, and (ii) the properties of magnetic minerals are temperature dependent, we carried out additional magnetic measurements to address the temperature-dependence of our results. These ancillary measurements are described in the appendix.

3. Measurements results

Scanning SQUID data were acquired by taking discrete measurements of magnetic flux at $1\ \mu\text{m}$ intervals, about $1\ \mu\text{m}$ above the sample surface. For each sample, acquisition was completed on several rectangular areas: 3 areas of about $80 \times 80\ \mu\text{m}$ for sample 1, 13 areas of about $100 \times 300\ \mu\text{m}$ for sample 2, and 4 areas of about $100 \times 300\ \mu\text{m}$ for sample 3. For each sample, the image of the magnetic field was obtained by merging the individual areas and manually adjusting minor offsets along the edges due to small differences in sensor elevation.

The raw SQUID result for the reference sample 1 is shown in Fig. 3a. Little variation is observed, as expected for the reference quartz sand sample, except for some isolated dipolar features,

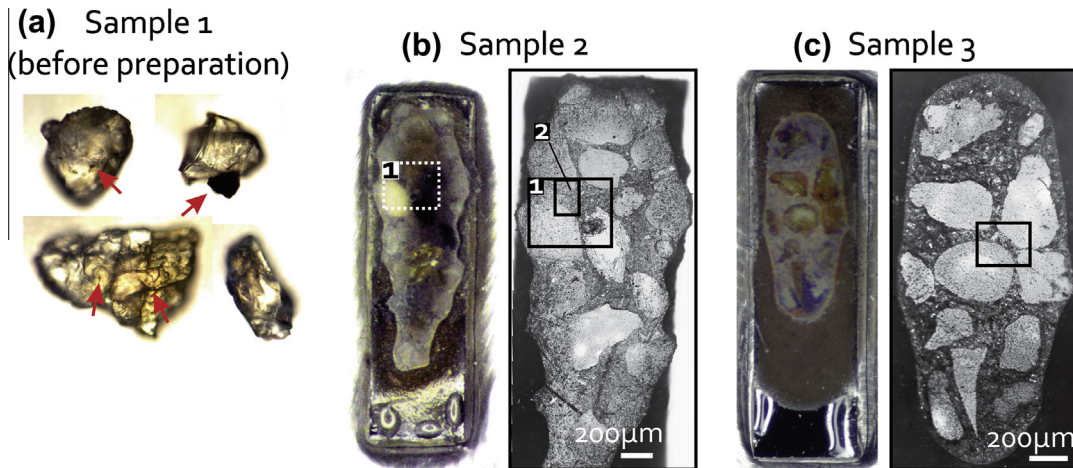


Fig. 2. Optical microscopy images of the three samples. (a) Sample 1 is the clean quartz sand, shown before polishing. Small black, potentially magnetic, grains are marked by the red arrows. (b) Two images of sample 2, composed of natural sand grains. Rectangle 1 shows the region measured by scanning SQUID microscopy. Rectangle 2 shows the region on which we focus our discussion. (c) Two images of sample 3, composed of quartz grains from natural sand. The rectangular area shows the region measured by scanning SQUID microscopy. The two images in (b) and (c) are a low-resolution color image (left) and a high resolution grayscale image. (For interpretation of the references to color in this figure legend, the reader is referred to the web version of this article.)

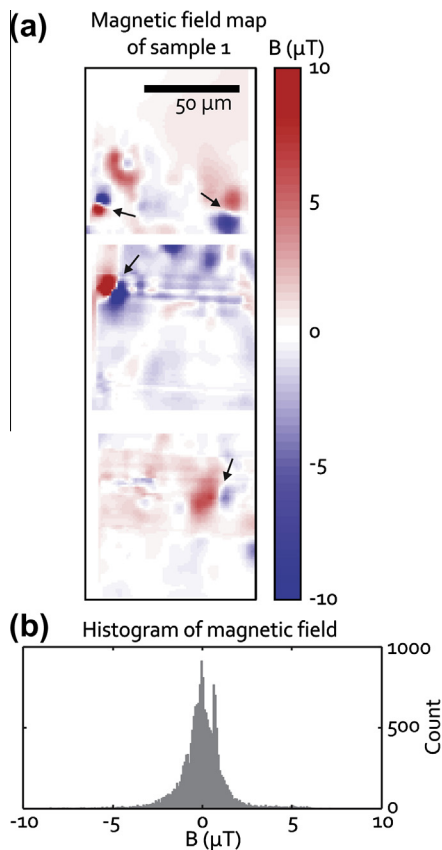


Fig. 3. (a) Raw magnetic field map of sample 1 (reference sample) obtained by scanning SQUID microscopy. Arrows highlight isolated dipolar features. (b) Histogram of the magnetic field values shown in (a).

which we attribute to small magnetic grains such as the ones marked by the arrows in Fig. 2a. The field distribution is roughly Gaussian, see Fig. 3b.

The raw SQUID result for sample 2 is shown in Fig. 4. This region, covered by scanning SQUID, is marked on the optical microscopy image by rectangle 1 in Fig. 2b. The magnetic image is dominated by a large-scale dipolar feature with a magnetic field

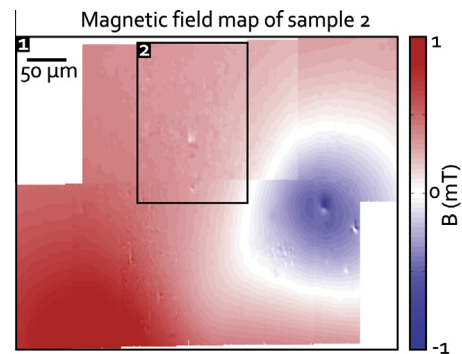


Fig. 4. Raw magnetic field map of sample 2 (rectangle 1 in Fig. 2b) obtained from scanning SQUID microscopy. Image is assembled from 13 patches; field values of patches are adjusted manually to correct for DC offset between the images. Numbered rectangular areas correspond to the rectangles in Fig. 2b.

varying from about 1 mT at the lower left corner to about -1 mT at the right edge. Comparison of Fig. 2b and Fig. 4 suggests that the field variation is likely due to the black grain (presumed to be magnetite).

In order to examine magnetic features that occur on a smaller scale, we apply a Gaussian filter to remove the dominating dipolar feature from the magnetic field map of sample 2. This process is illustrated in Fig. 5, displaying the region marked by rectangle 2 in Fig. 2b and Fig. 4. We chose a diameter of $23 \mu\text{m}$ for the Gaussian filter to remove features of longer spatial correlation length. The filtered image shown in Fig. 5b is a much smoother version of the raw image in Fig. 5a. By subtracting the filtered image from the raw image, we obtain an image that emphasizes small-scale variations, as shown in Fig. 5c.

We show again rectangle 2, in Fig. 6a the microscopy image and in Fig. 6b the magnetic image, but here restricted to a magnetic field variation of $30 \mu\text{T}$ peak-to-peak amplitude. We identified the grain boundaries by comparing Fig. 6a and b. The main part of the image is pore space, appearing as darker-colored¹ region in Fig. 6a. The upper left and lower left parts of the image are occupied by grains, indicated by the brighter colors in Fig. 6a. In the magnetic

¹ For interpretation of color in Figs. 6 and 7, the reader is referred to the web version of this article.

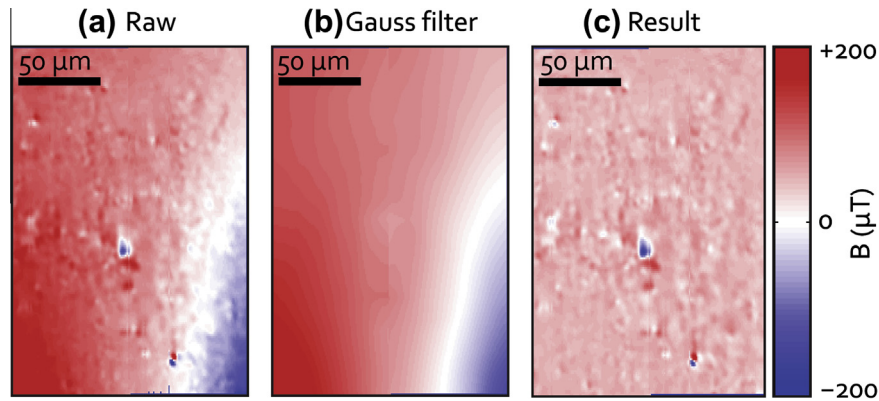


Fig. 5. SQUID results from sample 2 (rectangle 2 in Fig. 2b). (a) Raw magnetic field map is dominated by strong dipolar feature extending from lower left to lower right corner. (b) Magnetic map after applying a Gaussian filter with a diameter of 23 μm . (c) Subtracting filtered map in (b) from raw map in (a) results in map that emphasizes small scale magnetic features. Scale bar in all images is 50 μm .

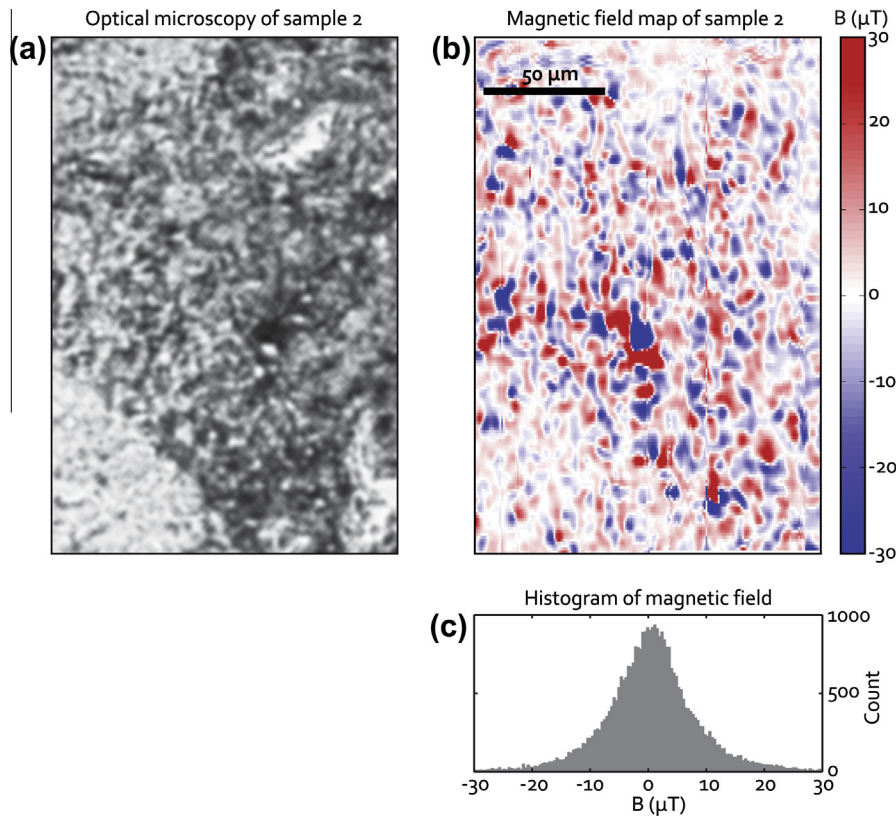


Fig. 6. (a) Optical microscopy image of sample 2 (rectangle 2 in Fig. 2b). Brighter regions mark grains, darker regions mark pore space. (b) Magnetic field map corresponding to (a) after Gaussian filter. (c) Histogram of the magnetic field values shown in (b).

map we observe large variations on a small spatial scale throughout the pore space. At the grain boundaries we observe pronounced field variations, exceeding 60 μT over short distances of 10 μm . The grains appear as fainter areas in the magnetic image, indicating less magnetic variation within the grains. The field distribution follows a Gaussian characteristic, as shown in Fig. 6c.

The results after Gaussian filtering for the pore space region of sample 3, marked by the rectangular area in Fig. 2c, are shown in Fig. 7. As for Fig. 6, we show in Fig. 7a the optical microscopy image where grains appear as brighter colors and the pore space as darker colors, and in Fig. 7b the corresponding magnetic image. We observe a similar structure in the magnetic field map as for sample 2: field variations are pronounced in the pore space and at the grain boundaries. Less variation is observed within the grains.

The field distribution follows a Gaussian characteristic, as shown in Fig. 7c. The magnitude of the field variations is about 20 μT over short distances of 10 μm . The variation is smaller than for sample 2, but still substantial.

4. Discussion

For the reference sample 1 we observed relatively little variation of the internal field, as shown by the smooth field map in Fig. 3a. Exceptions are isolated dipolar features, marked by black arrows in Fig. 3a. Because quartz is generally nonmagnetic, we attribute these features to trace magnetic components in the sample.

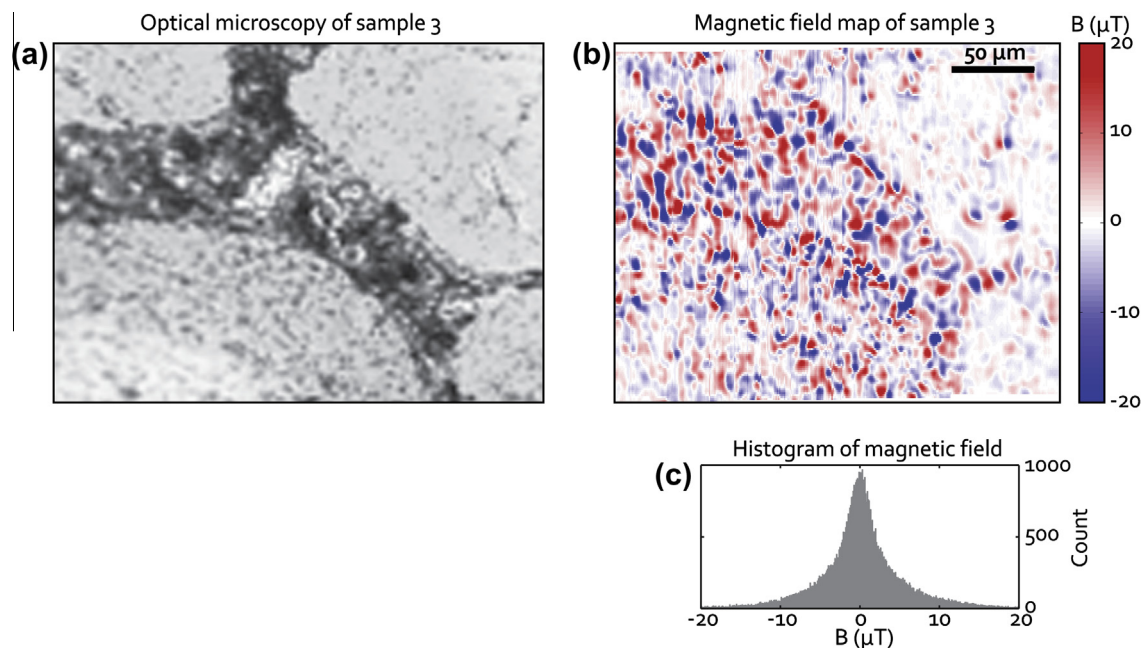


Fig. 7. (a) Optical microscopy image of sample 3 (rectangle in Fig. 2c). Brighter regions mark grains, darker regions mark pore space. (b) Magnetic field map of sample 3 after Gaussian filter. This area is marked by the rectangle in Fig. 2c. Dashed lines indicate grain boundaries. (c) Histogram of the magnetic field values shown in (b).

We observed major internal field variations in the natural samples. The variations occur on different spatial scales: (i) relatively large-scale variations of about 2 mT over 200 μm , as observed in the unfiltered data for sample 2 (Fig. 4), that are due to the presence of the black (presumed magnetic) grain; (ii) small-scale variations of about 20–30 μT over short distances of 10 μm , as observed in the filtered data for samples 2 and 3 (Fig. 6b and Fig. 7b, respectively) that we attribute to the presence of very fine magnetic grains. The observed variations are substantial, considering that the measurements were acquired at very low background field (~ 2 μT). The observed variations are much larger than expected from the assumptions commonly made in NMR that magnetic variations scale with the background magnetic field. Because we observed the variations at low background field, we conclude that they are not induced by the background field and magnetic susceptibility contrasts, but occur due to remanent magnetization.

After applying a Gaussian filter to remove magnetic features occurring on large spatial scale, we observed pronounced internal field variations along the pore surfaces. But we also observed substantial variations within the pore space. Since we worked in a clean nonmagnetic environment, and the potential sources of magnetic contamination are much weaker than our magnetic signal, the only possible explanation for these variations within the pore space is that very fine-grained magnetic material, part of the starting sample, went into the pore space when we mixed the grains and the epoxy during sample preparation. In situ, the fine-grained material would occur either adsorbed to the surfaces of bigger grains, or in suspension in the pore water, thus giving rise to magnetic variations. SQUID measurements were taken on samples at a temperature of 4 K. To assess how well we can transfer our results to experiments at room temperature, we made control measurements monitoring the temperature dependence of sample magnetization. More details of the measurements are given in Appendix A. We observed that for samples obtained from the same material as scanning-SQUID sample 2, the magnitude of magnetization varied by less than one order of magnitude when cooled from room temperature to 4 K. From this we conclude that our scanning SQUID results provide estimates of internal field variations that are valid at room temperature within one order of magnitude.

The observed substantial internal field variations have the potential to severely influence NMR studies of natural porous material. Considering Earth field NMR, the observed field variations are larger than the background field. This would invalidate the assumption commonly made on the initial condition in an Earth field NMR experiment that in thermal equilibrium the proton spins of the pore fluid are aligned along Earth's field axis. This could lead to parts of the fluid-filled pore space not being excited in an NMR experiment, and therefore not properly accounted for when estimating porosity. Similarly, considering that excitation pulses in low-field experiments can be relatively long and thus frequency selective, such large variations could lead to the Larmor frequency in some regions of the pore space being shifted out of the excitation bandwidth of pulses. These effects could lead to substantial underestimation of water content. In NMR relaxometry experiments aimed at measuring the T_2 relaxation time it is often assumed that the effect of relaxation due to diffusion through field gradients can be minimized by selecting a short echo time. But to suppress internal field gradients of the order of 1 T/m as observed here, might necessitate echo times of less than 1 ms, which is difficult to achieve. In pulsed-field-gradient measurements to determine restricted diffusion coefficients, the internal fields could dominate externally applied gradients, leading to misinterpretation of measured diffusion processes. In imaging experiments the strong internal gradients could distort spatial phase and frequency encoding, leading to voxel misplacement in image reconstruction. In most of the described scenarios it would be difficult to remove the effect of the internal fields, because their orientation and magnitude is unknown. Our results provide important data needed to better understand the magnitude of magnetic field variations that occur in natural porous media. The results can be used to estimate the potential effect on NMR experiments, or develop strategies for mitigation.

5. Conclusions

Understanding the internal magnetic fields is essential for characterizing porous materials by NMR. In this study we demonstrate

that prior assumptions made about internal fields of natural porous materials may be invalid. We measured the internal fields of sand grains extracted from natural geologic samples employing scanning SQUID microscopy, an excellent method to directly quantify internal fields due to its outstanding sensitivity to magnetic fields. Even though we carried out our measurements in a very low background of 2 μT (only about 1/25 of Earth's field), we found substantial internal magnetic field variations. We detected a variation of more than 2 mT across the relatively long spatial scale of 200 μm , induced by large magnetic grains. We also detected pronounced small-scale variations that occurred mainly along pore surfaces, with variations exceeding 60 μT over the small range of 10 μm , which we attribute to very fine-grained magnetic material. Because our measurements were conducted at very low background field, we conclude that the observed variations are not induced by the background field, but due to natural remanent magnetization carried by magnetic particles. While the magnitude of the observed field variations is much larger than predicted, its distribution is roughly Gaussian, as commonly assumed.

Our results demonstrate that substantial internal magnetic field variation can be present in natural geologic material, even at low background fields such as Earth's field. These natural internal field variations can potentially lead to biased NMR measurements of water content, relaxation times, or restricted diffusion. In the future, we plan to use our measurement results in numerical simulations of NMR experiments to quantify the impact of the large observed magnetic field variations on common NMR experiments to determine porosity and pore size.

Acknowledgments

We thank Eric Spanton for his support with the SQUID measurements, and the Fisher lab at Stanford for their support with measurements to determine the temperature dependence of magnetic moment. JW was supported by a grant from the National Science Foundation (Grant No. 0911234). BK was supported by EC Grant No. FP7-PEOPLE-2012-CIG-333799, FENA-MARCO Contract No. 0160SMB958, DARPA No. C10J10834, and NSF DMR-0803974. The scanning SQUID measurement technique was developed with support from the NSF-sponsored Center for Probing the Nanoscale at Stanford, NSF-NSEC 0830228, and NSF IMR-MIP 0957616. The measurements of temperature dependence were carried out on a MPMS system, Quantum Design Inc., California, US. The synthetic sand used for the reference sample was obtained from Wedron Silica Co., Illinois, US. We thank the anonymous reviewers for their comments that helped improve this manuscript.

Appendix A. Temperature dependence of magnetization

The purpose of our scanning SQUID measurements is to estimate the magnitude of internal field variations caused by remanent magnetization of magnetic particles in natural porous media at room temperature. Scanning SQUID measurements, however, are taken on samples cooled to a temperature of about 4 K. The magnetic properties of materials are temperature dependent, and it is therefore important to assess how the magnetic properties changed when we cooled our samples from room temperature to 4 K. Generally, the temperature dependence of magnetic properties is a function of the magnetic mineral's composition, grain size, and grain shape. For example, one study found that for samples of small-grained magnetite ($\sim 1 \mu\text{m}$), the saturation remanent magnetization obtained at 1 T was reduced to about 50% of its initial value at room temperature [66]. It is difficult to theoretically predict the temperature dependence for our natural samples, because we do not know the exact compositions, sizes, and shapes of all

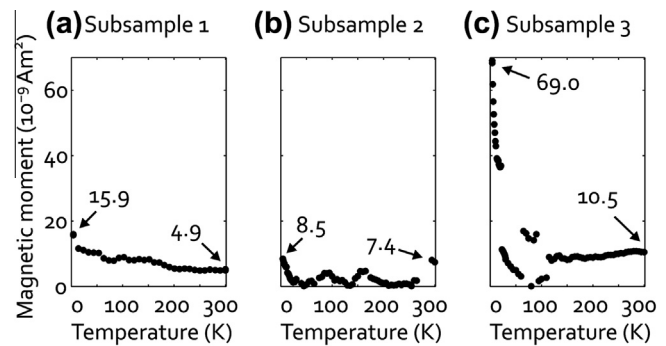


Fig. A.1. Magnetic moment of three subsamples of mass 0.12 g, 0.06 g, and 0.18 g (a–c) of sample 2, measured during cooling the samples from room temperature to 4 K. Arrows indicate the values of magnetic moment at the start of the temperature sweep at room temperature and at the end of temperature sweep at 4 K. Error bars are smaller than symbol size.

grains in the sample. To get an estimate of the temperature dependence, we measured one component of the magnetic moment of three subsamples obtained from the same material as sample 2, using a commercial magnetometer (Quantum Design MPMS). The samples had cylindrical shape with radius 0.5 cm, height ~ 0.5 cm, and masses of 0.12 g, 0.06 g, and 0.18 g. We note that we measured magnetic moment instead of magnetization (i.e., magnetic moment per volume), because we did not determine the exact volume of our sample material. But since the sample volume did not change between measurements, our results are equally valid for sample magnetization.

The results of the measurements are shown in Fig. A.1. For subsample 1, the magnitude of magnetization increased by a factor of 3 during cooling, from about 5 $\text{A m}^2/\text{vol.}$ at room temperature to 16 $\text{A m}^2/\text{vol.}$ at 4 K, see Fig. A.1a. For subsample 2, the magnetization varied within 1 order of magnitude, with a small overall magnitude increase of 13% from $\sim 7.4 \text{ A m}^2/\text{vol.}$ at room temperature to $\sim 8.5 \text{ A m}^2/\text{vol.}$ at 4 K, see Fig. A.1a. For subsample 3, we observed a slight linear decrease in magnetization magnitude between room temperature and about 120 K, see Fig. A.1c. At temperatures below 120 K the increase in magnitude is more pronounced. Overall the magnitude of magnetization increased by a factor 7, from 10.5 $\text{A m}^2/\text{vol.}$ at room temperature to 69.0 $\text{A m}^2/\text{vol.}$ at 4 K.

The measurements of magnetization are taken on a much larger scale (cm-scale) than our scanning SQUID measurements (μm -scale). Still these results can be used as a rough guideline for the temperature dependence of the small-scale internal field variations that we probe with our SQUID measurements. We thus conclude that, within one order of magnitude, the internal fields we measure at 4 K by scanning SQUID microscopy are valid estimates for room temperature settings.

References

- [1] Y.-Q. Song, H. Cho, T. Hopper, A.E. Pomerantz, P.Z. Sun, Magnetic resonance in porous media: recent progress, *J. Chem. Phys.* 128 (2008) 052212-1–052212-12.
- [2] M. Hertrich, Imaging of groundwater with nuclear magnetic resonance, *Prog. Nucl. Magn. Reson. Spectrosc.* 53 (2008) 227–248.
- [3] J.A. Lehmann-Horn, J.O. Walbrecker, M. Hertrich, G. Langston, A.F. McClymont, A.G. Green, Imaging groundwater beneath a rugged proglacial moraine, *Geophysics* 76 (2011) B165–B172.
- [4] K. Chalikhakis, M.R. Nielsen, A. Legchenko, T.F. Hagensen, Investigation of sedimentary aquifers in Denmark using the magnetic resonance sounding method (MRS), *C. R. Geosci.* 341 (2009) 918–927.
- [5] S. Costabel, U. Yaramanci, Relative hydraulic conductivity in the vadose zone from magnetic resonance sounding—Brooks–Corey parameterization of the capillary fringe, *Geophysics* 76 (2011) G61–G71.
- [6] E. Grunewald, R. Knight, A laboratory study of NMR relaxation times in unconsolidated heterogeneous sediments, *Geophysics* 76 (2011) G73–G83.

- [7] A. Legchenko, J. Baltassat, A. Bobachev, C. Martin, H. Robain, J.-M. Vouillamoz, Magnetic resonance sounding applied to aquifer characterization, *Groundwater* 42 (2004) 363–373.
- [8] R. Knight, E. Grunewald, T. Irons, K. Dlubac, Y.-Q. Song, H.N. Bachman, et al., Field experiment provides ground truth for surface nuclear magnetic resonance measurement, *Geophys. Res. Lett.* 39 (2012) 1–7.
- [9] K. Dlubac, R. Knight, Y.-Q. Song, N. Bachman, B. Grau, J. Cannia, et al., Use of NMR logging to obtain estimates of hydraulic conductivity in the High Plains aquifer, Nebraska, USA, *Water Resour. Res.* 49 (2013) 1–16.
- [10] R. Kleinberg, Pore size distributions, pore coupling, and transverse relaxation spectra of porous rocks, *Magn. Reson. Imaging* 12 (1994) 271–274.
- [11] K. Packer, Oil reservoir rocks examined by MRI, in: *Encycl. Magn. Reson.*, John Wiley & Sons Ltd., 2007, pp. 1–12.
- [12] C. Straley, D. Rossini, H.J. Vinegar, P. Tutunjian, C. Morriss, Core analysis by low-field NMR, *Log Anal.* 38 (1997) 84–94.
- [13] R. Freedman, N. Heaton, M. Flaum, G. Hirasaki, Wettability, saturation, and viscosity from NMR measurements, *SPE J.* 8 (2003) 317–327.
- [14] J. Howard, W. Kenyon, Determination of pore size distribution in sedimentary rocks by proton nuclear magnetic resonance, *Mar. Pet. Geol.* 9 (1992) 139–145.
- [15] J.V. Bayer, F. Jaeger, G.E. Schaumann, Proton Nuclear Magnetic Resonance (NMR) relaxometry in soil science applications, *Open Magn. Reson. J.* 3 (2010) 15–26.
- [16] T.R. Bryar, R.J. Knight, NMR relaxation measurements to quantify immiscible organic contaminants in sediments, *Water Resour. Res.* 44 (2008). W02401-1–W02401-12.
- [17] A. Pohlmeier, S. Haber-Pohlmeier, S. Stapf, A fast field cycling nuclear magnetic resonance relaxometry study of natural soils, *Vadose Zone J.* 8 (2009) 735–742.
- [18] F. Jaeger, S. Bowe, H. Van As, G.E. Schaumann, Evaluation of 1 H NMR relaxometry for the assessment of pore-size distribution in soil samples, *Eur. J. Soil Sci.* 60 (2009) 1052–1064.
- [19] T.R. Todoruk, C.H. Langford, A. Kantzas, Pore-scale redistribution of water during wetting of air-dried soils as studied by low-field NMR relaxometry, *Environ. Sci. Technol.* 37 (2003) 2707–2713.
- [20] R. Hertzog, T. White, C. Straley, Using NMR decay-time measurements to monitor and characterize DNAPL and moisture in subsurface porous media, *J. Environ. Eng. Geophys.* 12 (2007) 293–306.
- [21] C.H. Arns, Y.H. Melean, A.P. Sheppard, M.A. Knackstedt, A comparison of pore structure analysis by NMR and X-ray-CT techniques, in: *SPWLA 49th Annu. Logging Symp.*, SPWLA, 2008, pp. 1–13.
- [22] K. Brownstein, C. Tarr, Importance of classical diffusion in NMR studies of water in biological cells, *Phys. Rev. A* 19 (1979) 2446–2453.
- [23] B. Sun, K.-J. Dunn, Methods and limitations of NMR data inversion for fluid typing, *J. Magn. Reson.* 169 (2004) 118–128.
- [24] M. Hürlimann, D. Freed, L. Zielinski, Y.-Q. Song, G. Leu, C. Straley, et al., Hydrocarbon composition from NMR diffusion and relaxation data, *Petrophysics* 50 (2009) 116–129.
- [25] M. Hürlimann, L. Venkataraman, C. Flaum, The diffusion–spin relaxation time distribution function as an experimental probe to characterize fluid mixtures in porous media, *J. Chem. Phys.* 117 (2002) 10223–10232.
- [26] L. Latour, P. Mitra, R.L. Kleinberg, C.H. Sotak, Time-dependent diffusion coefficient of fluids in porous media as a probe of surface-to-volume ratio, *J. Magn. Reson., Ser. A* 101 (1993) 342–346.
- [27] P.N. Sen, Time-dependent diffusion coefficient as a probe of geometry, *Concepts Magn. Reson.* 23A (2004) 1–21.
- [28] M. Hürlimann, K. Helmer, L.L. Latour, C.H. Sotak, Restricted diffusion in sedimentary rocks. Determination of surface-area-to-volume ratio and surface relaxivity, *J. Magn. Reson., Ser. A* 111 (1994) 169–178.
- [29] I. Mitreiter, S.E. Oswald, F. Stallmach, Investigation of iron(III)-release in the pore water of natural sands by NMR relaxometry, *Open Magn. Reson. J.* 3 (2010) 46–51.
- [30] R.J.S. Brown, Distribution of fields from randomly placed dipoles: free-precession signal decay as result of magnetic grains, *Phys. Rev.* 121 (1961) 1379–1382.
- [31] P.N. Sen, S. Axelrod, Inhomogeneity in local magnetic field due to susceptibility contrast, *J. Appl. Phys.* 86 (1999) 4548–4554.
- [32] M. Hürlimann, Effective gradients in porous media due to susceptibility differences, *J. Magn. Reson.* 131 (1998) 232–240.
- [33] V. Anand, G.J. Hirasaki, Paramagnetic relaxation in sandstones: distinguishing T1 and T2 dependence on surface relaxation, internal gradients and dependence on echo spacing, *J. Magn. Reson.* 190 (2008) 68–85.
- [34] B. Audoly, P.N. Sen, S. Ryu, Y.-Q. Song, Correlation functions for inhomogeneous magnetic field in random media with application to a dense random pack of spheres, *J. Magn. Reson.* 164 (2003) 154–159.
- [35] Q. Chen, A.E. Marble, B.G. Colpitts, B.J. Balcom, The internal magnetic field distribution, and single exponential magnetic resonance free induction decay, in rocks, *J. Magn. Reson.* 175 (2005) 300–308.
- [36] J.N. Morelli, V.M. Runge, F. Ai, U. Attenberger, L. Vu, S. Schmeets, et al., An image-based approach to understanding the physics of MR artifacts, *Radiographics* 31 (2011) 849–867.
- [37] D. Grebenkov, Use, misuse, and abuse of apparent diffusion coefficients, *Concepts Magn. Reson. Part A* (2010) 24–35.
- [38] J. Mitchell, T.C. Chandrasekera, M.L. Johns, L.F. Gladden, E.J. Fordham, Nuclear magnetic resonance relaxation and diffusion in the presence of internal gradients: the effect of magnetic field strength, *Phys. Rev. E* 81 (2010) 026101-1–026101-19.
- [39] H. Carr, E. Purcell, Effects of diffusion on free precession in nuclear magnetic resonance experiments, *Phys. Rev.* 94 (1954) 630–638.
- [40] J. Petković, H.P. Huinink, L. Pel, K. Kopinga, Diffusion in porous building materials with high internal magnetic field gradients, *J. Magn. Reson.* 167 (2004) 97–106.
- [41] R.F. Karlicek, I.J. Lowe, A modified pulsed gradient technique for measuring diffusion in the presence of large background gradients, *J. Magn. Reson.* 37 (1980) 75–91.
- [42] R. Cotts, M. Hoch, T. Sun, J. Markert, Pulsed field gradient stimulated echo methods for improved NMR diffusion measurements in heterogeneous systems, *J. Magn. Reson.* 83 (1989) 252–266.
- [43] P.Z. Sun, J.G. Seland, D. Cory, Background gradient suppression in pulsed gradient stimulated echo measurements, *J. Magn. Reson.* 161 (2003) 168–173.
- [44] P. Galvosas, F. Stallmach, J. Kärgler, Background gradient suppression in stimulated echo NMR diffusion studies using magic pulsed field gradient ratios, *J. Magn. Reson.* 166 (2004) 164–173.
- [45] G.H. Sørland, D. Aksnes, L. Gjerdåker, A pulsed field gradient spin-echo method for diffusion measurements in the presence of internal gradients, *J. Magn. Reson.* 137 (1999) 397–401.
- [46] Y.-Q. Song, S. Ryu, P.N. Sen, Determining multiple length scales in rocks, *Nature* 406 (2000) 178–181.
- [47] Y.-Q. Song, Pore sizes and pore connectivity in rocks using the effect of internal field, *Magn. Reson. Imaging* 19 (2001) 417–421.
- [48] Y.-Q. Song, Using internal magnetic fields to obtain pore size distributions of porous media, *Concepts Magn. Reson.* 18A (2003) 97–110.
- [49] E.E. Sigmund, H. Cho, P. Chen, S. Byrnes, Y.-Q. Song, X.E. Guo, et al., Diffusion-based MR methods for bone structure and evolution, *Magn. Reson. Med.* 59 (2008) 28–39.
- [50] E.E. Sigmund, H. Cho, Y.-Q. Song, High-resolution MRI of internal field diffusion-weighting in trabecular bone, *NMR Biomed.* 22 (2009) 436–448.
- [51] H.J. Cho, E.E. Sigmund, Y.-Q. Song, Magnetic resonance characterization of porous media using diffusion through internal magnetic fields, *Materials (Basel)* 5 (2012) 590–616.
- [52] K.J. Dunn, Magnetic susceptibility contrast induced field gradients in porous media, *Magn. Reson. Imaging* 19 (2001) 439–442.
- [53] M. Appel, J.J. Freeman, J.S. Gardner, G.H. Hirasaki, Q.G. Zhang, J.L. Shafer, Interpretation of restricted diffusion in sandstones with internal field gradients, *Magn. Reson. Imaging* 19 (2001) 535–537.
- [54] B. Sun, K.-J. Dunn, Probing the internal field gradients of porous media, *Phys. Rev. E* 65 (2002) 051309-1–051309-7.
- [55] K.E. Washburn, C.D. Eccles, P.T. Callaghan, The dependence on magnetic field strength of correlated internal gradient relaxation time distributions in heterogeneous materials, *J. Magn. Reson.* 194 (2008) 33–40.
- [56] H. Cho, S. Ryu, J.L. Ackerman, Y.-Q. Song, Visualization of inhomogeneous local magnetic field gradient due to susceptibility contrast, *J. Magn. Reson.* 198 (2009) 88–93.
- [57] M. Winkler, M. Zhou, M. Bernardo, B. Endeward, H. Thomann, Internal magnetic gradient fields in glass bead packs from numerical simulations and constant time diffusion spin echo measurements, *Magn. Reson. Imaging* 21 (2003) 311–315.
- [58] L.J. Burnett, J.A. Jackson, Remote (inside-out) NMR. II. Sensitivity of NMR detection for external samples, *J. Magn. Reson.* 41 (1980) 406–410.
- [59] G. Zhang, G. Hirasaki, W. House, Internal field gradients in porous media, *Petrophysics* 44 (2003) 422–434.
- [60] B.W. Gardner, J.C. Wynn, P.G. Björnsson, E.W.J. Straver, K.A. Moler, J.R. Kirtley, et al., Scanning superconducting quantum interference device susceptometry, *Rev. Sci. Instrum.* 72 (2001) 2361–2364.
- [61] M.E. Huber, N.C. Koshnick, H. Bluhm, L.J. Archuleta, T. Azua, P.G. Björnsson, et al., Gradiometric micro-SQUID susceptometer for scanning measurements of mesoscopic samples, *Rev. Sci. Instrum.* 79 (2008) 053704-1–053704-7.
- [62] N.C. Koshnick, M.E. Huber, J.A. Bert, W. Hicks, J. Large, H. Edwards, et al., A terraced scanning superconducting quantum interference device susceptometer with sub-micron pickup loops, *Appl. Phys. Lett.* 93 (2008) 1–3.
- [63] B. Kalisky, J.A. Bert, B.B. Klopfer, C. Bell, H.K. Sato, M. Hosoda, et al., Critical thickness for ferromagnetism in LaAlO₃/SrTiO₃ heterostructures, *Nat. Commun.* 3 (2012) 922.
- [64] T.P. Irons, C.M. Hobza, G.V. Steele, J.D. Abraham, J.C. Cannia, D.D. Woodward, Quantification of Aquifer Properties with Surface Nuclear Magnetic Resonance in the Platte River Valley, Central Nebraska, Using a Novel Inversion Method, *U.S. Geol. Surv. Sci. Investig. Sci. Investig. Rep.* 2012–5189 (2012) 1–51.
- [65] M.E. Evans, F. Heller, *Enviromagnetic minerals*, in: *Environ. Magn. Princ. Appl. Enviromagnetics*, Academic Press, San Diego, 2001, pp. 31–49.
- [66] J.G. King, W. Williams, Low-temperature magnetic properties of magnetite, *J. Geophys. Res.* 105 (2000) 16427–16436.